Check for updates

Insights into isothiourea-catalyzed asymmetric [3 + 3] annulation of α,β-unsaturated aryl esters with 2-acylbenzazoles: mechanism, origin of stereoselectivity and switchable chemoselectivity†

Congcong Wang, [iD]ᵃ Shi-Jun Li, [iD]ᵇ Qiao-Chu Zhang,ᵇ Donghui Wei [iD]*ᵇ and Lina Ding [iD]*ᵃ

Recently, isothiourea-catalyzed asymmetric [3 + 3] annulation reactions of α,β-unsaturated aryl esters with 2-acylbenzothiazole (or 2-acylbenzoxazole) were reported with switchable chemoselectivity to form either dihydropyridone or dihydropyranone, but predicting the origin of chemoselectivity and stereoselectivity is still challenging in these kinds of reactions. Herein, density functional theory (DFT) was used to study the general mechanism and explore the origin of stereoselectivity and chemoselectivity in these reactions. The calculated results show that three stages including adsorption, [3 + 3] annulation and dissociation are involved in the reaction, and the C–C bond formation involved in [3 + 3] annulation is a key step that determines both chemoselectivity and stereoselectivity. The origin of stereoselectivity was further investigated by analysis of distortion and non-covalent interactions (NCI), and the C–H···O interaction between the chiral substituents of the catalyst and the carbonyl oxygen on 2-acylbenzazoles contributes greatly to the stereoselectivity. In addition, the switchable chemoselectivity associated with the competitive [3 + 3] cyclizations for formation of *N*- and *O*-heterocyclic compounds can be predicted by using local nucleophilic Parr function (P_k^-) and nucleophilic atom energy (E_a^-) analysis. This work provides guidance for the rational design of potential catalysts for such highly stereoselective reactions with switchable chemoselectivities.

Introduction

Functionalized six-membered ring compounds such as pyridone and pyranone are important building blocks for synthesis of pharmaceutical drugs and natural products.[1] Catalytic stereoselective access to these kinds of ring compounds has thus attracted considerable research interest. Various kinds of efficient pathways were reported to synthesize these cyclic compounds, such as the common [4 + 2] cycloaddition and the emerging [3 + 3] cyclization reaction. For these synthesis processes, the use of a suitable catalyst will result in a convenient reaction associated with mild

ᵃ *Collaborative Innovation Center of New Drug Research and Safety Evaluation, Henan Province, Key Laboratory of Technology of Drug Preparation (Zhengzhou University), Ministry of Education of China, Key Laboratory of Henan Province for Drug Quality and Evaluation, School of Pharmaceutical Sciences, Zhengzhou University, Zhengzhou 450001, P. R. China. E-mail: dinglina123@126.com*

ᵇ *College of Chemistry, and Institute of Green Catalysis, Zhengzhou University, 100 Science Avenue, Zhengzhou 450001, Henan, P. R. China.
E-mail: donghuiwei@zzu.edu.cn*
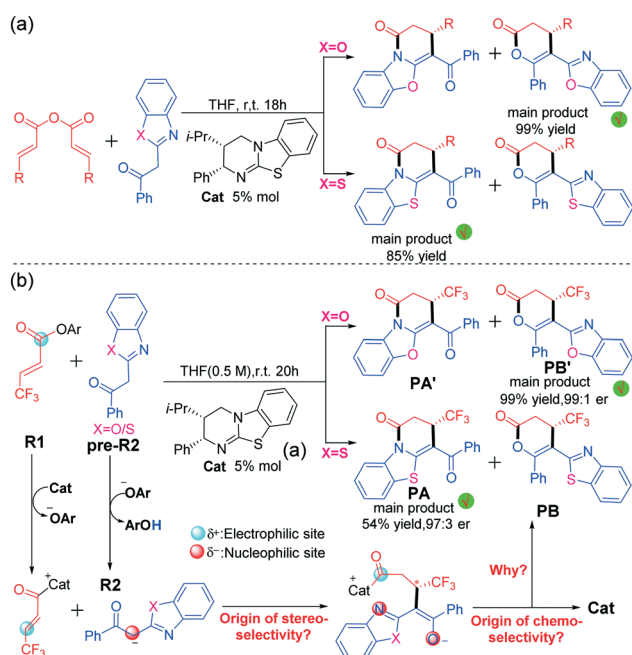
Scheme 1 Isothiourea-catalysed [3 + 3] annulation reaction of (a) homoanhydrides with 2-acylbenzazole derivatives and (b) α,β-unsaturated aryl esters with 2-acylbenzazole.

3664 | *Catal. Sci. Technol.*, 2020, **10**, 3664–3669

This journal is © The Royal Society of Chemistry 2020

conditions and high selectivity.[2] Noteworthily, the employment of Lewis base organocatalysts,[3] including cinchona alkaloid derivatives,[4] N-heterocyclic carbenes,[5] phosphine,[6] and isothiourea,[7] was found to be an ideal choice for promoting various kinds of asymmetric syntheses of those N- and O-heterocyclic compounds.[8]

More recently, the use of chiral isothioureas[9] has become more and more popular in enantioselective synthesis of six-membered ring compounds. Notably, Smith et al. widely extended their applications to build many complex compounds with high levels of regio-, chemo- and stereo-control capabilities. Besides isothiourea-catalyzed [4 + 2] cyclization reactions for formation of various six-membered ring compounds,[10] Smith's group reported the isothiourea-catalyzed [3 + 3] cyclization reaction of 2-acylbenzoxazoles with homo-anhydrides to form dihydropyranone and dihydropyridinone (Scheme 1a).[11,12] Moreover, Smith et al. reported the isothiourea-catalyzed formal [3 + 3] cyclization reaction of 2-acylbenzoxazole with α,β-unsaturated aryl esters to generate dihydropyranone and dihydropyridinone, which has good stereoselectivity and chemoselectivity (Scheme 1b).[13] However, the origin of the chemoselectivity and stereoselectivity in these kinds of isothiourea-catalyzed [3 + 3] cyclization reactions remains unclear so far. As can be seen in Scheme 1a, the product is exclusively dihydropyranone when the **X** atom is an oxygen atom, but the main product would be dihydropyridinone when the **X** atom is a sulfur atom, and the yield ratio of dihydropyridinone : dihydropyranone is 85 : 15 in the experiment.[11] Similarly, as shown in Scheme 1b, similar products would be obtained and chemoselectivity can be switchable by using different substrates with **X** = **S** or **O** atoms.

Although there are a lot of valuable insights in these excellent experiments, some issues still need to be further studied and explored in theory: (1) how is an acyl ammonium precursor converted from an α,β-unsaturated aryl ester? (2) What is the role of the leaving group **ArO**⁻? (3) How does the deprotonation proceed to produce the corresponding enolate intermediate? (4) How do protonic media assist [1,3]-proton transfer? (5) What is the origin of high stereoselectivity? (6) What role does the isothiourea catalyst play? To the best of our knowledge, few theoretical studies on the isothiourea-catalyzed asymmetric [3 + 3] annulation of α,β-unsaturated aryl esters (or homoanhydrides) with 2-acylbenzazoles have been reported so far,[11] and the general principle on the origin of the switchable chemoselectivities and selectivities should be highly desirable to explore them systematically. These questions and our continuous interest in organocatalysis[14–16] encourage us to perform this computational study, in which the reactions of 3-trifluoromethyl-1-(2,4,6-trichlorophenoxy)-2-acetyl (denoted as **R1**, Scheme 1b) with 2-benzoxazole-1-acetophenone (denoted as **R2**$_{O/S}$ with X = O/S, Scheme 1b) leading to dihydropyridone and dihydropyranone in the presence of isothiourea (denoted as **Cat**) were selected as the research

object. All of the calculations were conducted at the M06-2X-D3/6-311++G(2df, 2pd)/IEF-PCM$_{THF}$//M06-2X[17,18]/6-31G(d, p)/IEF-PCM$_{THF}$[19,20] level in the Gaussian 09 program,[21] and more computational details are provided in the ESI.† This theoretical study aims to explore the exact map for general mechanisms of such reactions, and thus provides valuable clues for guiding experimental design.

Results and discussion

Mechanism for the [3 + 3] cyclization

As shown in Scheme 2, we suggested and studied the possible mechanisms of [3 + 3] cyclization of an α,β-unsaturated aryl ester with 2-acylbenzothiazole catalyzed by isothiourea, and Fig. 1 shows the relative free energy profiles of the entire catalytic reaction, in which the free energy of **R1** + **Cat** was set to 0.0 kcal mol⁻¹. The entire catalytic cycle comprises four reaction steps, and we would elaborate on the specific mechanism and free energy change of each step as follows.

The first step is initiated with nucleophilic attack on the carbonyl carbon of reactant **R1** from either the **Si** or **Re** face of the carbonyl group of **R1** by the imine nitrogen atom of **Cat** via transition state **Si-** or **Re-TS1** to generate intermediate **Si-** or **Re-M1** (Fig. S1 of the ESI†). For convenience, the unchanged chirality of the catalyst has not been included in the names of the following stationary points including the diastereomer intermediates and transition states. It should be noted that the chirality of the catalyst was not mentioned in the compound names. The **Si-** or **Re-**before the compound names corresponds to the **Si-** or **Re-**face of reactant **R1**, and the same signs for the associated **Si-** or **Re-M1** were retained. As seen from Fig. 1, the energy barrier of the pathway associated with attacking the **Re** surface of the carbonyl group of reactant **R1** through transition state **Re-TS1** (13.0 kcal mol⁻¹) is lower than that via **Si-TS1** (14.4 kcal mol⁻¹). In addition, the energy of intermediate **Re-M1** (−0.1 kcal mol⁻¹)

Scheme 2 The competitive reaction mechanisms for the isothiourea-catalyzed [3 + 3] annulation of an α,β-unsaturated aryl ester with 2-acylbenzothiazole.
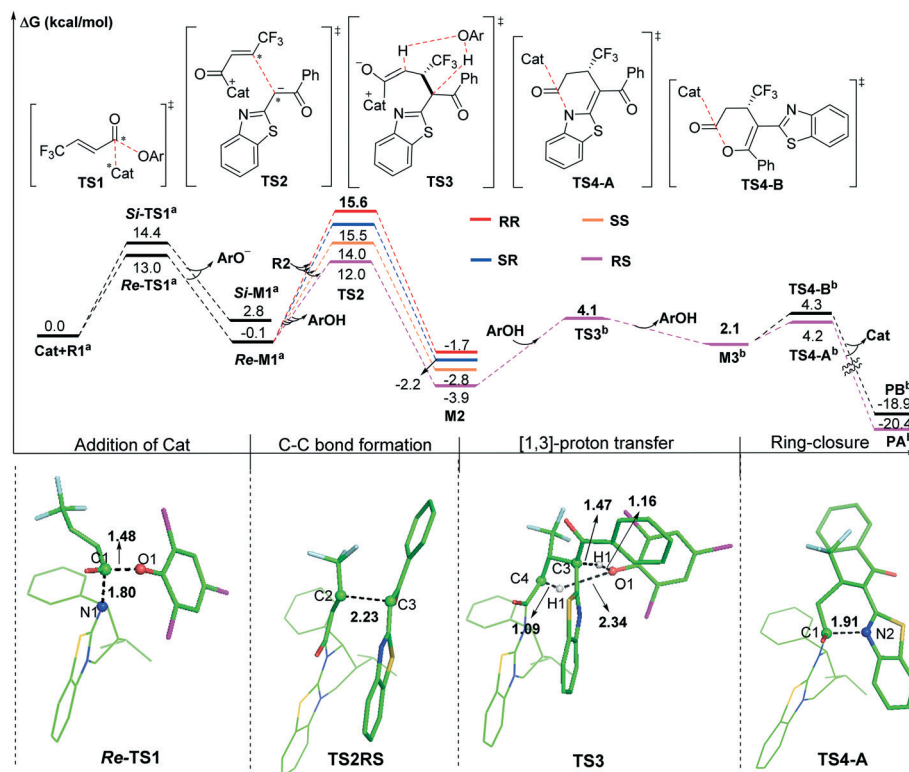
This journal is © The Royal Society of Chemistry 2020

Catal. Sci. Technol., 2020, **10**, 3664–3669 | **3665**

Fig. 1 The relative Gibbs free energy profiles of the isothiourea-catalyzed [3 + 3] annulation reaction. (the superscript "a" represents adding the free energy of **pre-R2**, the superscript "b" represents the *S* configuration, and distances are in angstroms).

is also lower than that of *Si*-**M1** (2.8 kcal mol^{−1}). Therefore, the pathway associated with *Re*-**M1** should be more energetically favourable in both kinetics and thermodynamics, so we only considered this pathway in the following steps.

The second step is Michael addition to **M1** by nucleophile **R2**, which is generated *via* the α-C–H deprotonation process of reactant precursor **pre-R2** in the presence of **ArO**[−] through transition state **TS1'** (7.4 kcal mol^{−1}, Fig. S2 of the ESI†). It should be noted that a molecule of **ArOH** can be generated to assist the following [1,3]-proton transfer. In this step, α-C of **R2** attacks the activated α-C of intermediate **M1** to form intermediate **M2** *via* transition state **TS2**. As shown in Scheme 1, there are two nucleophilic sites on **R2**, namely α-C and the oxygen atom of the carbonyl group. In order to explore which atom is easier to attack to form intermediate **M1**, local nucleophilic (P_k^-) and electrophilic (P_k^+) Parr function analysis[22] was performed for **R2**, and the calculated results indicated that nucleophilicity of α-C is much greater than that of the carbonyl oxygen atom (Table S1 of the ESI†). Furthermore, we analysed the global reaction index (GRI[23]) to understand the actual role of the isothiourea catalyst. As shown in Table S2 of the ESI,† the **ArO**[−] can be nucleophilically substituted by isothiourea, which makes the substrate more electrophilic to facilitate the reaction with nucleophile **R2**.

As shown in Fig. 2, four different reaction modes would lead to the corresponding diastereoisomer transition states,

i.e. **TS2*SS***, **TS2*RS***, **TS2*RR*** and **TS2*SR***. According to Fig. 1, the energy barriers *via* transition states **TS2*SS***, **TS2*RS***, **TS2*RR*** and **TS2*SR*** are 14.0, 12.0, 15.6 and 15.5 kcal mol^{−1}, and the relative energies of the corresponding intermediates **M2*SS***, **M2*RS***, **M2*RR*** and **M2*SR*** are −2.8, −3.9, −1.7 and −2.2 kcal mol^{−1}, respectively. These data indicate that the reaction pathway for generating intermediate **M2*RS*** *via* **TS2*RS*** requires much lower energy than the other three pathways,

Fig. 2 Stereochemistry involved in transition states **TS2*SS***, **TS2*RS***, **TS2*RR*** and **TS2*SR***.

3666 | *Catal. Sci. Technol.*, 2020, **10**, 3664–3669

This journal is © The Royal Society of Chemistry 2020

so the reaction pattern for generating the **RS** isomer is more advantageous. Noteworthily, we considered and studied multiple conformations for transition state **TS2** to make sure that the selected conformations of the diastereoisomers are the lowest energy conformations, and more details can be found in Table S3 in the ESI.†

In third step, two possible pathways, including *in situ* generated **ArOH** and **i-Pr₂NEt·H⁺** assisted [1,3]-proton transfer *via* transition states **TS3** (with an energy barrier of 2.5 kcal mol⁻¹, Fig. 1) and **TS3′** (with an energy barrier of 23.2 kcal mol⁻¹, Fig. S3 of the ESI†), were considered and investigated. Obviously, the **ArOH** assisted [1,3]-proton transfer has a much lower energy barrier and should be the main pathway in the reaction.

The final step is ring closure coupled with dissociation of **Cat** for formation of either product **PA** or **PB** *via* transition state **TS4-A** or **TS4-B** (Scheme 2), separately. As seen from Fig. 1, the energy barrier *via* transition state **TS4-A** (4.2 kcal mol⁻¹) is slightly lower than that *via* transition state **TS4-B** (4.3 kcal mol⁻¹), and the relative energy of product **PA** is also lower than that of product **PB**, which is in agreement with the product ratio (**PA**:**PB** = 54:42) obtained in the experiment. In contrast, for **X** = **O** shown in Fig. S4 of the ESI,† the energy barrier *via* transition state **TS4-B′** (4.5 kcal mol⁻¹) is much lower than that *via* transition state **TS4-A′** (11.3 kcal mol⁻¹), the relative energy of product **PB′** (−12.8 kcal mol⁻¹) is higher than that of product **PA′** (−19.7 kcal mol⁻¹), and **PA′** should be the kinetically-unfavoured but thermodynamically-favoured product, which is consistent with the main product being changed to **PA′** under heating conditions. The calculated results are consistent with the observed switchable chemoselectivity in the experiment, and this interesting phenomenon encouraged us to further explore the origin of chemoselectivity as follows.[24]

Origin of stereoselectivity

According to the energy barrier diagram (Fig. 1) and above discussed in step 2, the Michael addition was identified as the stereoselectivity-determining step, and the reaction pathway associated with the **RS** configuration has the lowest energy. The energy difference between **TS2RS** and **TS2SR** is 3.5 kcal mol⁻¹, which corresponds to 99% ee in theory, and this is close to the 94% ee reported in experiment. In order to explore the origin of stereoselectivity, the distortion/interaction energy[25] and non-covalent interaction (NCI) analyses were performed as follows.

Based on Houk's definition,[25,26] the energy difference between the reaction partners (**M1** and **R2**) and the corresponding segments separated from each transition state ($\Delta E^{\ddagger}_{\text{dist\_M1}}/\Delta E^{\ddagger}_{\text{dist\_R2}}$) is the distortion energy, and the total distortion energy ($\Delta E^{\ddagger}_{\text{dist\_total}}$) is the sum of $\Delta E^{\ddagger}_{\text{dist\_M1}}$ and $\Delta E^{\ddagger}_{\text{dist\_R2}}$. The weak interaction $\Delta E^{\ddagger}_{\text{int}}$ is the difference between $\Delta E^{\ddagger}$ and $\Delta E^{\ddagger}_{\text{dist\_total}}$. As summarized in Table 1, although the transition state **TS2RS** has the largest distortion energy (15.45 kcal mol⁻¹), it also has the largest interaction energy (−38.63

Table 1 The relative distortion/interaction energy analysis for the stereocontrolling transition states calculated at the M06-2X-GD3/6-31++G (2df, 2pd)/IEF-PCM$_{\text{THF}}$ level (unit: kcal mol⁻¹)

SP	$\Delta\Delta G^{\ddagger}$	$\Delta E^{\ddagger}_{\text{dist\_R2}}$	$\Delta E^{\ddagger}_{\text{dist\_M1}}$	$\Delta E^{\ddagger}_{\text{dist\_total}}$	$\Delta E^{\ddagger}_{\text{int}}$
TS2SS	1.93	4.32	8.67	12.99	−33.20
TS2RS	0.00	4.69	11.01	15.70	−37.27
TS2RR	3.52	2.49	6.92	9.41	−28.38
TS2SR	3.48	1.68	7.89	9.57	−26.74

kcal mol⁻¹), indicating that the weak interactions contribute significantly for its favourability. Therefore, we further performed non-covalent interaction (NCI) analysis on transition states **TS2SS**, **TS2RS**, **TS2RR** and **TS2SR** to discover those interactions. Several kinds of interactions have been identified by using NCI analysis, *i.e.* lp···π interaction, C–H···O interaction, C–H···S interaction, and C–H···π interaction. Noteworthily, the lone pair···π (lp···π) interaction is similar to the anion···π interaction, namely the non-covalent bonding association between a neutral electron-rich atom and an electron-poor π ring.[27] As depicted in Fig. 3, there are one lp···π interaction (2.97 Å) between carbonyl oxygen and the five-membered ring and one lp···π interaction (3.31 Å) between the sulfur atom and the six-membered ring in **TS2SS**; one lp···π interaction (2.94 Å) between the carbonyl oxygen and the five-membered ring, one C–H···S interaction (2.91 Å) and one strong C–H···O interaction (2.34 Å) in **TS2RS**; one lp···π interaction (2.98 Å) between the carbonyl oxygen and the five-membered ring and one lp···π interaction (3.17 Å) between the sulfur atom and the six-membered ring in **TS2RR**, one C–H···π interaction (2.45 Å), one C–H···S interaction (2.99 Å) and one C–H···O interaction (2.59 Å) in **TS2SR**. Therefore, the stronger C–H···O interaction between **R2** and the chiral center of the catalyst in transition state **TS2RS** should be the key to determine the stereoselectivity of the reaction.

Fig. 3 Stereochemistry involved in transition states **TS2SS**, **TS2RS**, **TS2RR** and **TS2SR**.
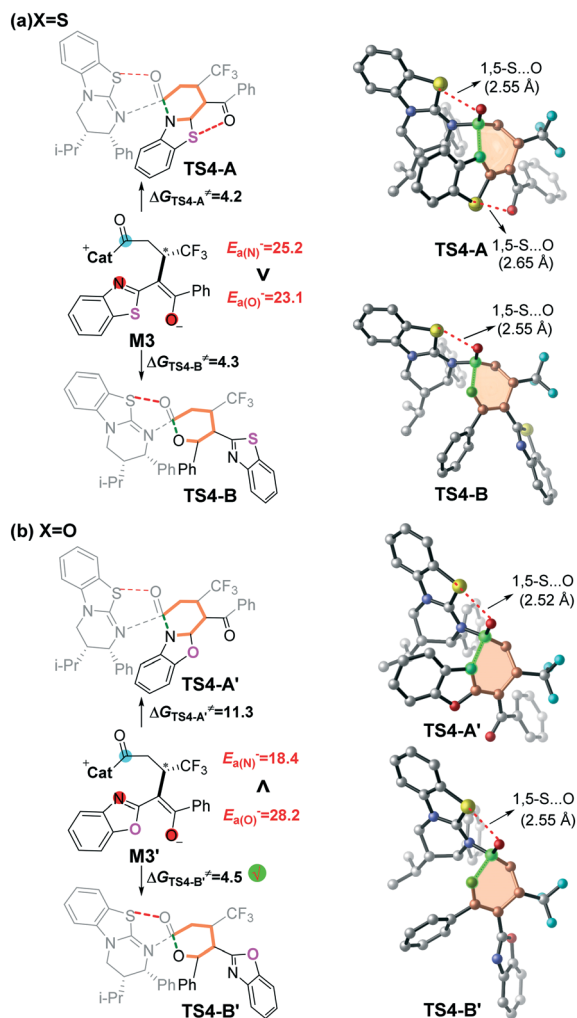
This journal is © The Royal Society of Chemistry 2020

Catal. Sci. Technol., 2020, **10**, 3664–3669 | **3667**

Fig. 4 Nucleophilic atom energy (E_a^-, kcal mol^{-1}) of N and O atoms in intermediates **M3** and **M3'**.

Prediction of chemoselectivity

Inspired by Smith's excellent contribution,[11,28–30] we think that it should be interesting to explore the origin of the switchable chemoselectivity. Noteworthily, the number of 1,5-S···O interactions could be used for explaining the chemoselectivity involved in this kind of reaction depicted in Fig. 4a. However, as shown in Fig. 4b, the two chemoselective transition states have only one 1,5-S···O interaction, so the switchable chemoselectivity cannot be well explained so far.

In order to predict the chemoselectivity associated with [3 + 3] cyclization products **PA** or **PB** by using a general principle, we determined the global nucleophilic index (N (ref. 23d and 31 = $E_{\text{HOMO (M3, M3')}}$ − $E_{\text{HOMO (TCNE)}}$) of intermediate **M3** or **M3'** and local nucleophilicity (P_k^-), and performed nucleophilic atom energy ($E_a^- = P_k^- \times N$) analyses on the nucleophilic nitrogen and oxygen atoms in intermediate **M3** or **M3'** (Table S4 of the ESI†). The computed results (Fig. 4) show that the nucleophilicity of the nitrogen atom ($E_a^- = 25.2$ kcal mol^{-1}) is slightly higher than that of the

oxygen atom ($E_a^- = 23.1$ kcal mol^{-1}) in intermediate **M3**. While the nucleophilicity of the nitrogen atom ($E_a^- = 18.4$ kcal mol^{-1}) is significantly lower than that of the oxygen atom ($E_a^- = 28.2$ kcal mol^{-1}) in intermediate **M3'**. The higher nucleophilic atom energy represents the stronger nucleophilic activity, and thus leads to a lower energy barrier. Therefore, we can successfully predict the switchable chemoselectivity by performing single-point energy calculations according to the above two local reactivity indexes.

Conclusions

In this work, density functional theory (DFT) calculations were carried out to study the possible reaction mechanisms and origin of selectivities of the reaction between α,β-unsaturated aryl esters and 2-acylbenzazole (**X** = **O/S**) to generate dihydropyridone and dihydropyranone under isothiourea organocatalysis. The calculated results reveal that the reaction includes four reaction steps, including complexation of α,β-unsaturated aryl esters using the isothiourea catalyst, Michael addition, **ArOH** assisted [1,3]-proton transfer, and the ring-closure process coupled with dissociation of the catalyst. The Michael addition step (*i.e.* C–C bond formation) was identified as the stereoselectivity-determining step. Analysis of the distortion/interaction and non-covalent interaction (NCI) shows that the C–H···O interaction formed between the two chiral centers on the catalyst with the carbonyl oxygen on 2-acylbenzothiazole has a significant influence on the stereoselectivity. In addition, analysis of a newly suggested local activity index (*i.e.* nucleophilic atom energy E_a^-) and nucleophilic Parr function (P_k^-) was performed to predict the origin of the switchable chemoselectivity in these kinds of reactions. Therefore, this work should be helpful in understanding the detailed reaction mechanism, role of the isothiourea organocatalyst, and origin of both stereoselectivity and chemoselectivity, and thus provides useful clues for rational design of more efficient organocatalyzed [3 + 3] cyclization reactions with high stereoselectivity and special chemoselectivity.

Conflicts of interest

There are no conflicts to declare.

Acknowledgements

Notes and references

1 C. G. Hui, F. Chen, F. Pu and J. Xu, *Nat. Rev. Chem.*, 2019, **3**, 85–107.

2 J. P. Page and T. V. RajanBabu, *J. Am. Chem. Soc.*, 2012, **134**, 6556–6559.

3 C. Guo, M. Fleige, D. Janssen-Meller, C. G. Daniliuc and F. Glorius, *Nat. Chem.*, 2015, **7**, 842–847.

4 (*a*) L. Jiang and Y. C. Chen, *Catal. Sci. Technol.*, 2011, **1**, 354; (*b*) P. Melchiorre, *Angew. Chem., Int. Ed.*, 2012, **51**, 9748.

5 (*a*) H. U. Vora, P. Wheeler and T. Rovis, *Adv. Synth. Catal.*, 2012, **354**, 1617; (*b*) S. J. Ryan, L. Candish and D. W. Lupton, *Chem. Soc. Rev.*, 2013, **42**, 4906.

6 W. Wang, Y. Wang, L. J. Zheng, Y. Qiao and D. H. Wei, *ChemistrySelect*, 2017, **2**, 5266–5273.

7 T. H. West, D. M. Walden, J. E. Taylor, A. C. Brueckner, R. C. Johnston, P. H. Y. Cheong, G. C. L. Jones and A. D. Smith, *J. Am. Chem. Soc.*, 2017, **139**, 4366–4375.

8 (*a*) D. G. Stark, L. C. Morrill, P.-P. Yeh, A. M. Z. Slawin, T. J. C. ORiordan and A. D. Smith, *Angew. Chem., Int. Ed.*, 2013, **52**, 11642–11646; (*b*) S. L. Wang, J. Izquierdo, C. R. Escrich and M. A. Pericàs, *ACS Catal.*, 2017, **7**, 2780–2785.

9 B. V. Birman and X. Li, *Org. Lett.*, 2006, **8**, 1351–1354.

10 S. L. Wang, J. Izquierdo, C. Rodriguez-Escrich and M. A. Pericàs, *ACS Catal.*, 2017, **7**, 2780.

11 E. R. T. Robinson, D. M. Walden, C. Fallan, M. D. Greenhalgh, P. H.-Y. Cheong and A. D. Smith, *Chem. Sci.*, 2016, **7**, 6919–6927.

12 For a review on isothiourea catalysis see: (*a*) J. Merad, J.-M. Pons, O. Chuzel and C. Bressy, *Eur. J. Org. Chem.*, 2016, **2016**, 5589–5610; (*b*) C. Joannesse, C. P. Johnson, C. Concellon, C. Simal, D. Philp and A. D. Smith, *Angew. Chem., Int. Ed.*, 2009, **48**, 8914–8918; (*c*) C. A. Leverett, V. C. Purohit and D. Romo, *Angew. Chem., Int. Ed.*, 2010, **49**, 9479–9483; (*d*) D. Belmessieri, L. C. Morill, C. Simal, A. M. Z. Slawin and A. D. Smith, *J. Am. Chem. Soc.*, 2011, **133**, 2714–2720.

13 M. D. Greenhalgh, S. Qu, A. M. Z. Slawin and A. D. Smith, *Chem. Sci.*, 2018, **9**, 4909.

14 (*a*) Y. Y. Wang, D. H. Wei, Y. Wang, W. J. Zhang and M. S. Tang, *ACS Catal.*, 2016, **6**, 279–289; (*b*) S. Li, Z. W. Tang, Y. Wang, D. Wang, Z. L. Wang, C. X. Yu, T. J. Li, D. H. Wei and C. S. Yao, *Org. Lett.*, 2019, **21**, 1306–1310.

15 (*a*) X. K. Guo, L. B. Zhang, D. H. Wei and J. L. Niu, *Chem. Sci.*, 2015, **6**, 7059–7071; (*b*) K. Sun, S. J. Li, X. L. Chen, Y. Liu, X. Q. Huang, D. H. Wei, L. B. Qu, Y. F. Zhao and B. Yu, *Chem. Commun.*, 2019, **55**, 2861–2864.

16 (*a*) D. H. Wei, B. L. Lei, M. S. Tang and C.-G. Zhan, *J. Am. Chem. Soc.*, 2012, **134**, 10436–10450; (*b*) D. H. Wei, X. Q. Huang, Y. Qiao, J. J. Rao, L. Wang, F. Liao and C.-G. Zhan, *ACS Catal.*, 2017, **7**, 4623–4636.

17 Y. Zhao and D. G. Truhlar, *Theor. Chem. Acc.*, 2008, **120**, 215–241.

18 Y. Zhao and D. G. Truhlar, *Acc. Chem. Res.*, 2008, **41**, 157–167.

19 B. Mennucci and J. Tomasi, *J. Chem. Phys.*, 1997, **106**, 5151.

20 V. Barone and M. Cossi, *J. Phys. Chem. A*, 1998, **102**, 1995.

21 M. J. Frisch, G. W. Trucks, H. B. Schlegel, G. E. Scuseria, M. A. Robb, J. R. Cheeseman, G. Scalmani, V. Barone, B. Mennucci, G. A. Petersson, H. Nakatsuji, M. Caricato, X. Li, H. P. Hratchian, A. F. Izmaylov, J. Bloino, G. Zheng, J. L. Sonnenberg, M. Hada, M. Ehara, K. Toyota, R. Fukuda, M. Hada, M. Ehara, K. Toyota, R. Fukuda, J. Hasegawa, M. Ishida, T. Nakajima, Y. Honda, O. Kitao, H. Nakai, T. Vreven, J. A. Montgomery Jr., J. E. Peralta, F. Ogliaro, M. Bearpark, J. J. Heyd, E. Brothers, K. N. Kudin, V. N. Staroverov, R. Kobayashi, J. Normand, K. Raghavachari, A. Rendell, J. C. Burant, S. S. Iyengar, J. Tomasi, M. Cossi, N. Rega, J. M. Millam, M. Klene, J. E. Knox, J. B. Cross, V. Bakken, C. Adamo, J. Jaramillo, R. Gomperts, R. E. Stratmann, O. Yazyev, A. J. Austin, R. Cammi, C. Pomelli, J. W. Ochterski, R. L. Martin, K. Morokuma, V. G. Zakrzewski, G. A. Voth, P. Salvador, J. J. Dannenberg, S. Dapprich, A. D. Daniels, O. Farkas, J. B. Foresman, J. V. Ortiz, J. Cioslowski and D. J. Fox, *Gaussian 09, Revision C.01*, Gaussian, Inc., Wallingford, CT, 2010.

22 (*a*) L. R. Domingo, P. Pérez and J. A. Sáez, *RSC Adv.*, 2013, **3**, 1486–1494; (*b*) L. J. Zheng, Y. Wang, D. H. Wei and Y. Qiao, *Chem. – Asian J.*, 2016, **11**, 3046–3054.

23 (*a*) R. G. Parr and R. G. Pearson, *J. Am. Chem. Soc.*, 1983, **105**, 7512–7516; (*b*) W. Kohn and L. J. Sham, *Phys. Rev.*, 1965, **140**, A1133; (*c*) L. J. Sham and W. Kohn, *Phys. Rev.*, 1966, **145**, 561; (*d*) L. R. Domingo, E. Chamorro and P. Pérez, *Eur. J. Org. Chem.*, 2009, **2009**, 3036–3044; (*e*) L. R. Domingo and P. Pérez, *Org. Biomol. Chem.*, 2013, **11**, 4350–4358; (*f*) L. R. Domingo, J. A. Saéz, R. J. Zaragozá and M. Arnó, *J. Org. Chem.*, 2008, **73**, 8791–8799; (*g*) D. Yepes, J. S. Murray, P. Pérez, L. R. Domingo, P. Politzer and P. Jaque, *Phys. Chem. Chem. Phys.*, 2014, **16**, 6726–6734.

24 (*a*) N. Liu, Y. F. Xie, C. Wang, S. J. Li, D. H. Wei and Bin Dai, *ACS Catal.*, 2018, **8**, 9945–9957; (*b*) Q. Q. Shi, W. Wang, Y. Wang, Y. Lan, C. S. Yao and D. H. Wei, *Org. Chem. Front.*, 2019, **6**, 2692; (*c*) Q. C. Zhang, X. Li, X. H. Wang, S. J. Li, L. B. Qu, Y. Lan and D. H. Wei, *Org. Chem. Front.*, 2019, **6**, 679–687.

25 (*a*) R. Gordillo and K. N. Houk, *J. Am. Chem. Soc.*, 2006, **128**, 3543–3553; (*b*) C. D. Anderson, T. Dudding, R. Gordillo and K. N. Houk, *Org. Lett.*, 2008, **10**, 2749–2752; (*c*) O. Gutierrez, R. G. Iafe and K. N. Houk, *Org. Lett.*, 2009, **11**, 4298–4301; (*d*) M. A. M. Capozzi, C. Centrone, G. Fracchiolla, F. Naso and C. Cardellicchio, *Eur. J. Org. Chem.*, 2011, 4327–4334.

26 F. M. Bickelhaupt and K. N. Houk, *Angew. Chem., Int. Ed.*, 2017, **56**, 10070–10086.

27 (*a*) D. Quinoñero, C. Garau, C. Rotger, A. Frontera, P. Ballester, A. Costa and P. M. Deya, *Angew. Chem., Int. Ed.*, 2002, **41**, 3389–3392; (*b*) T. J. Mooibroek, P. Gamez and J. Reedijk, *CrystEngComm*, 2008, **10**, 1501–1515.

28 C. Shu, H. L. Liu, A. M. Z. Slawin, C. Carpenter-Warrena and A. D. Smith, *Chem. Sci.*, 2020, **11**, 241–247.

29 T. H. West, D. M. Walden, J. E. Taylor, A. C. Brueckner, R. C. Johnston, P. H. Y. Cheong, G. C. L. Jones and A. D. Smith, *J. Am. Chem. Soc.*, 2017, **139**, 4366–4375.

30 D. J. B. Antúnez, M. D. Greenhalgh, A. C. Brueckner, D. M. Walden, P. E. Rodríguez, P. Roberts, B. G. Young, T. H. West, A. M. Z. Slawin, P. H. Y. Cheong and A. D. Smith, *Chem. Sci.*, 2019, **10**, 6162–6173.

31 (*a*) L. R. Domingo, E. Chamorro and P. Perez, *J. Phys. Chem. A*, 2008, **112**, 4046–4053; (*b*) L. R. Domingo and P. Perez, *Org. Biomol. Chem.*, 2011, **9**, 7168–7175.

This journal is © The Royal Society of Chemistry 2020

Catal. Sci. Technol., 2020, **10**, 3664–3669 | **3669**